Lawrence Berkeley National Laboratory

Title

Enhancement of Parametric Effects in Polariton Waveguides Induced by Dipolar Interactions

Permalink

https://escholarship.org/uc/item/5s82w65m

Authors

Suárez-Forero, DG
Riminucci, F
Ardizzone, V
et al.

Localization dynamics in a centrally coupled system

Nathan Ng,[1] Sebastian Wenderoth,[2] Rajagopala Reddy Seelam ©,[2] Eran Rabani,[3,4,5] Hans-Dieter Meyer,[6]
Michael Thoss,[2,7] and Michael Kolodrubetz[8]

[1]*Department of Physics, University of California, Berkeley, California 94720, USA*
[2]*Institute of Physics, University of Freiburg, Hermann-Herder-Strasse 3, 79104 Freiburg, Germany*
[3]*Department of Chemistry, University of California, Berkeley, California 94720, USA*
[4]*Materials Sciences Division, Lawrence Berkeley National Laboratory, Berkeley, California 94720, USA*
[5]*The Sackler Center for Computational Molecular and Materials Science, Tel Aviv University, Tel Aviv 69978, Israel*
[6]*Theoretische Chemie, Physikalisch-Chemisches Institut, Universität Heidelberg, INF 229, D-69120 Heidelberg, Germany*
[7]*EUCOR Centre for Quantum Science and Quantum Computing, University of Freiburg,*
Hermann-Herder-Strasse 3, 79104 Freiburg, Germany
[8]*Department of Physics, The University of Texas at Dallas, Richardson, Texas 75080, USA*

In systems in which interactions couple a central degree of freedom and a bath, one would expect signatures of the bath's phase to be reflected in the dynamics of the central degree of freedom. This has been recently explored in connection with many-body localized baths coupled with a central qubit or a single-cavity mode—systems with growing experimental relevance in various platforms. Such models also have an interesting connection with Floquet many-body localization via quantizing the external drive, although this has been relatively unexplored. Here we adapt the multilayer multiconfigurational time-dependent Hartree (ML-MCTDH) method, a well-known tree tensor network algorithm, to numerically simulate the dynamics of a central degree of freedom, represented by a d-level system (qudit), coupled to a disordered interacting one-dimensional spin bath. ML-MCTDH allows us to reach $\approx 10^2$ lattice sites, a far larger system size than what is feasible with exact diagonalization or kernel polynomial methods. From the intermediate time dynamics, we find a well-defined thermodynamic limit for the qudit dynamics upon appropriate rescaling of the system-bath coupling. The spin system shows similar scaling collapse in the Edward-Anderson spin-glass order parameter or entanglement entropy at relatively short times. At longer timescales, we see slow growth of the entanglement, which may arise from dephasing mechanisms in the localized system or long-range interactions mediated by the central degree of freedom. Similar signs of localization are shown to appear as well with unscaled system-bath coupling.

I. INTRODUCTION

The advent of controllable quantum simulation platforms allows for novel explorations of quantum coherent phenomena. Certain such architectures have the advantage of using extra degrees of freedom as a way to easily read out properties of a system [1]. Examples of such setups include cavity QED with ultracold atoms [2] and superconducting qubit circuits, the latter of which was recently used to simulate the many-body localized (MBL) phase in a 10-qubit chain with long-range interactions mediated by a central resonator [3]. Given that such platforms are in their early stages, it is important to explore the interplay of disorder-induced localization and mediated long-range interactions, and how they affect the dynamics of localization in these systems.

If localization exists in these systems, it will naturally be many-body localization since the spins hybridize with the central degree of freedom to give nontrivial interactions. Rigorous results on MBL have already been established in one-dimensional (1D) systems with short-ranged interactions [4]. In such a setting, it is a stable phase of matter, with respect to adding short-range perturbations, that can coexist

with other types of order [5,6]. While strong disorder enables localization, it cannot prevent thermalization if interactions are long-ranged, decaying slower than r^{-2D}, where D is the spatial dimension [7,8]. Even the MBL phase with short-ranged interactions is fragile. It is destroyed upon coupling to a continuum of bath modes [9], which, intuitively, can provide arbitrary amounts of energy and allow the system to transition between eigenstates of vastly different character. One sees then that there are two ingredients to this delocalization mechanism: a continuum of energies of large enough bandwidth, and hybridization due to effective infinite-ranged interactions mediated by the non-Markovian bath.

In fact, for a specific type of memoryless bath, nonergodicity does survive. This is the case of Floquet MBL, in which an MBL system is subjected to an external periodic drive with frequency Ω modeled as a time-dependent Hamiltonian acting on the system [10,11]. The failure of thermalization is due to the inability of the system to absorb energy in quanta of $\hbar\Omega$, which itself is a consequence of the discreteness of the energy spectrum. The external drive, however, is not inherently dynamical and thus does not capture the backaction present in a fully quantum-mechanical system.

In this work, we consider the time evolution of such a system obtained by treating the Floquet drive as a quantum degree of freedom. Specifically, we consider a localized system globally coupled to a d-level system (qudit) with finite energy spacing, similar to [12]. When the qudit is a two-level system, it was shown that localization does not survive at any finite coupling [13,14]. But when it is instead a $d > 2$ level system, localization was argued to survive under certain conditions [12]. It is not known, however, what dynamical signatures should be expected in such regimes since the geometry and spin-spin interactions in the system limit the efficiency of usual computational approaches using matrix product operators. We bridge this gap by numerically simulating the nonequilibrium dynamics at much larger system sizes than previously considered. This is done using the multilayer-multiconfigurational time-dependent Hartree (ML-MCTDH) method, which solves the Schrödinger equation using the time-dependent variational principle on the manifold of wave functions represented by certain tree tensor networks [15–19].

We furthermore explore the possibility that the additional degree of freedom can provide alternative, nondestructive diagnostics of localization. In experimental settings, the usual observables signaling nonergodic behavior are correlation functions such as the occupation imbalance between odd and even sites of the lattice [20]. More sophisticated setups may attempt to perform tomographic measurements to reconstruct the reduced density matrix for a subsystem and show logarithmic growth of entanglement entropy [3], or to measure the energy spectrum of the system in order to retrieve energy level spacing statistics [21]. Though these metrics serve as gold standards in characterizing MBL, the latter two methods are difficult to scale with larger systems. In our model, since quantum fluctuations of the spins necessarily involve the qudit, there may be signatures of (de)localization imprinted into the qudit dynamics. Such a possibility has been explored in autocorrelations of qudit observables [14] probing the energy level statistics, as well as dynamics of the occupation number [22] by measuring the light intensity output by a single mode cavity. In this work, we show that the qudit qualitatively changes the spin chain dynamics, and we elucidate the timescale on which this occurs. This provides some insight into the breakdown of localization, and the possible role that non-Floquet physics may play in it.

The structure of this paper is as follows: we will discuss our model and its localization in connection to Floquet MBL; review the essentials of ML-MCTDH, which we then apply to study intermediate time dynamics; present results on thermalizing and nonthermalizing behaviors in dynamical metrics; and discuss what may be expected in experiments, where control over the central coupling may be limited in range.

II. MODEL

We consider a simplified model of many-body localization by coupling a one-dimensional chain of qubits (spins-1/2) via global interactions with a central qudit:

$$H = H_0 + \Omega \hat{\tau}^z + \gamma H_1 (\hat{\tau}^+ + \text{H.c.}),$$

$$H_0 = \sum_{i=1}^{L} h\xi_i \sigma_i^z + g\sigma_i^z \sigma_{i+1}^z, \quad H_1 = \sum_{i=1}^{L} \sigma_i^x, \quad (1)$$

where $\hat{\tau}^z = \sum_{n=1}^{d} n|n\rangle\langle n|$, $\hat{\tau}^+ = \sum_{n=1}^{d-1} |n+1\rangle\langle n|$, and the operators H_0 and H_1 act only on the spin subspace. The states $|n\rangle$ label the states of the central qudit. Here, $h = 1.3$, $g = 1.07$, $\Omega = \pi/0.8$, and ξ_i is a random variable drawn uniformly from $(-1, 1)$. These parameters are chosen to be rather generic, with Ω large but finite, such that the model exhibits a numerically sharp localization-delocalization transition in the Floquet limit $d \to \infty$. The transition is signaled by adjacent level statistic $r = \min(\Delta E_{i,i+1}, \Delta E_{i-1,i})/\max(\Delta E_{i,i+1}, \Delta E_{i-1,i})$ and the bipartite entanglement entropy of eigenstates near the middle of the many-body spectrum. The position of this transition is at a critical coupling $\gamma_c \lesssim 0.3$ [23]. We restrict our discussion to γ either deep in the localized phase ($\gamma < 0.2$) or deep in the ergodic phase ($\gamma \approx 1$). Finally, throughout this paper we restrict ourselves to central qudit size $d = 7$, which is large enough to display Floquet-like behavior but small enough that the finite qudit size plays an important role.

The spin part of the Hamiltonian, H_0, is a trivial antiferromagnetic Ising chain with longitudinal on-site disorder. It can be alternatively conceptualized as a special case of the l-bit Hamiltonian for MBL systems in which only nearest-neighbor coupling remains and is uniform. The presence of the Ising coupling allows the spins to interact with each other independently of the qudit. The diagonal nature of H_0 in the z-basis yields trivial localization in the eigenstates. This manifests in eigenstates $|\psi_n\rangle$ as vanishing site-averaged magnetization $L^{-1} \sum_i \langle\psi_n|\sigma_i^z|\psi_n\rangle$ and the maximal value of the spin-glass parameter, $q = L^{-1} \sum_i \langle\psi_n|\sigma_i^z|\psi_n\rangle^2 = 1$, at high energy densities. Values of $q \approx 1$ suggest that the eigenstates are described mostly by a single pattern of magnetization. Introducing a small coupling to the qudit without longitudinal disorder induces hybridizations that push $q \to 0$. We find that it is necessary to have both qudit coupling and strong disorder to preserve the nonergodicity when probing the system in the middle of the many-body spectrum, where the density of states (DOS) is the greatest.

Several features distinguish our model from those studied previously. While Nandkishore et al. [9] coupled a "fully MBL" system to an interacting bath of bosons, the qudit we present here is not bathlike because it does not have a continuous DOS. The model of thermal inclusions studied by Ponte et al. [13] closely resembles ours, but crucially we place a constant "magnetic field" $\Omega \hat{\tau}_z$ on the qudit, thus selecting a preferred direction for the central spin. This greatly impacts the ease with which the qudit fluctuates, which in turn can regulate transitions in the spin states leading to delocalization.

Recent studies have examined how localization can persist in the presence of long-ranged interactions [8,22] or with central coupling to a single degree of freedom yielding an effective Hamiltonian with long-ranged interactions [13,14]. With the exception of a numerical study [22], these past works have noted that preservation of localization in the thermodynamic limit requires increasing the disorder strength with increasing system size or decreasing the strength of central coupling as $\gamma \to \gamma/L$. Reducing the coupling strength in this way renders the long-ranged part of the effective Hamiltonian for the spin chain subextensive. This is also reflected in the dynamics of the qudit as its transition rate vanishes.

On the other hand, the existence of Floquet MBL affords a different pathway to the coexistence of localization and central coupling. For our model, the mapping upon taking the Floquet limit, $d \to \infty$, gives a driven Hamiltonian

$$H_{\text{Floq}}(t) = \sum_{i=1}^{L} h\xi_i \sigma_i^z + g\sigma_i^z \sigma_{i+1}^z + 2\cos(\Omega t) \sum_{i=1}^{L} \sigma_i^x.$$

In this time-dependent context, the persistence of MBL is not due to a vanishing coupling to the external drive, but to a suppression of mixing between different localized eigenstates of the undriven system. This picture suggests that an effective Hamiltonian for only the spin degrees of freedom should show localized behavior. This is indeed the case, as previous work based on the high-frequency expansion has shown [12]. In this limit of $\Omega \to \infty$, the spins are governed by an effective Hamiltonian diagonal in the qudit basis, reproducing the eigenenergies modulo an integer multiple of Ω:

$$H_{\text{eff}} = H_0 + (H_1)^2 \frac{|d\rangle\langle d| - |1\rangle\langle 1|}{\Omega} + O(\Omega^{-2}). \quad (2)$$

At lowest order in Ω^{-1}, we see that possible delocalization is reserved only for states with $|1\rangle$ or $|d\rangle$, as $(H_1)^2$ induces all-to-all coupling. Increasing L without increasing d, as we do in this paper, means that eigenstates occupying $|1\rangle$ will eventually encroach upon the middle of the spectrum and contribute to the quench dynamics we study. This can be seen from the density of states when H_0 is dominant as it follows $\rho(E) \propto \exp\left(-\frac{E^2}{(J\sqrt{L})^2}\right)$ for the energy scale $J \sim O(1)$, meaning $\rho(E)$ will grow wider with increasing L. An energetically dominant $(H_1)^2$ term will both delocalize the eigenstates and deform the Gaussian density of states in the thermodynamic limit.

We thus assume γ to be small enough such that neither outcome occurs, and we ask when this picture will naively break down. In such a limit, we can treat the H_1^2 field term in a mean-field fashion for each eigenstate:

$$H_{\text{eff}} \approx H_0 + \frac{\gamma^2 L}{\Omega} + \sum_i \frac{\gamma^2}{\Omega} \left\langle \sum_{j\neq i} \sigma_j^x \right\rangle \sigma_i^x,$$

where the effective field $\langle \sum_{j\neq i} \sigma_j^x \rangle$ in an eigenstate must be determined self-consistently. For a typical eigenstate in the middle of the spectrum, this field should have the value $\sim f(\gamma)\sqrt{L}$, where $f(\gamma)$ must vanish when $\gamma = 0$. The transverse magnetization is subextensive at high energies where the density of states is dominated by contributions from the zero magnetization sector, allowing us to consider $\sum_j \langle \sigma_j^x \rangle$ to be the sum of $L - 1$ independent random variables with zero mean, and the finite γ eigenstates are assumed to be perturbatively connected to a corresponding $\gamma = 0$ eigenstate. For this model, we take the lowest-order approximation $f(\gamma) \approx f_1 \gamma$. With this assumption [24], the effective transverse field on site i will begin to compete with the longitudinal fields in H_0 when $\gamma^2 \langle \sum_{j\neq i} \sigma_j^x \rangle \sim O(g, h_i) \sim O(1)$. For the high-energy density eigenstates in which we are interested, this effective field will inhibit spin-glass ordering and the system should obey the eigenstate thermalization hypothesis. Thus, $\gamma \propto L^{-1/6}$ should serve as a rough separatrix between thermalizing and athermal behaviors. Furthermore, couplings that tend to zero faster
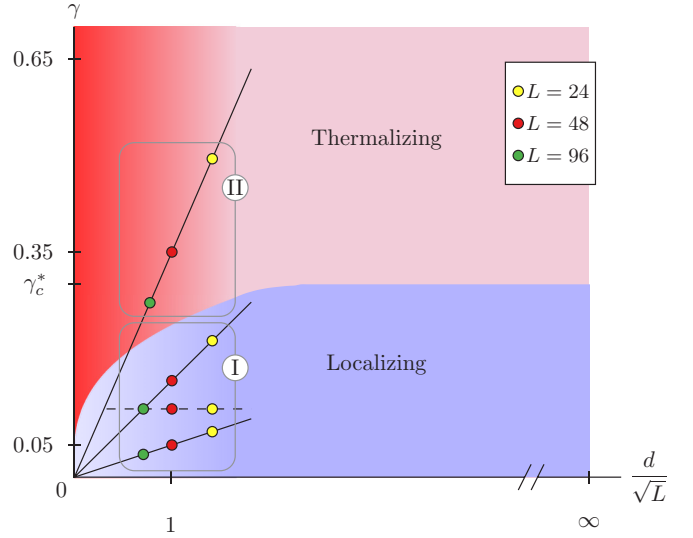

FIG. 1. Schematic phase diagram for the coupled system (1), along with the parameters for which we present numerical results from ML-MCTDH. The rough phase boundaries are determined from numerics and analytical arguments. The data are separated into three solid segments: the strong, intermediate, and weak couplings from top to bottom. The angle of the segments comes from fixing the qudit size to $d = 7$ and scaling the central coupling $\gamma \propto L^{-1/2}$. For ease of discussion, we group the three coupling regimes as region I (weak and intermediate) and region II (strong).

than $L^{-1/6}$ will realize a trivial limit, where the localization comes entirely from H_0. Note that, in general models where H_1 includes operators diagonal in the z-basis, we would have $f(0) \neq 0$; in this case, the scaling is replaced by $\gamma \sim L^{-1/4}$.

Besides scaling the coupling to zero, the all-to-all interactions can be avoided by ensuring that eigenstates occupying levels $|d\rangle$ or $|1\rangle$ in the qudit do not participate in the dynamics. For quenches starting from the middle of the many-body spectrum, this condition can be ensured by keeping the qudit size d sufficiently large compared to the typical width of the 1D many-body density of states, $\sqrt{L}$. The dynamics in this limit should closely resemble Floquet physics, since the fluctuations producing effective long-ranged interactions will cancel out after accounting for the processes in which the intermediate qudit state changes by $+1$ or -1. Away from this limit, when $d/\sqrt{L} \lesssim O(1)$, the all-to-all interactions are unavoidable. The threshold value of $d/\sqrt{L}$ for delocalization should decrease as the coupling is decreased. These arguments are summarized schematically in Fig. 1.

There are two important ways to think of this system and its dynamics: either as a combined many-body systems with localized and delocalized phases, as was done in the previous paragraph, or as a central qudit interacting with an unusual, localized, spin bath. From this latter viewpoint, it will be useful to consider scaling the system bath coupling $\gamma \sim 1/\sqrt{L}$, since that will be shown to achieve a well-defined thermodynamic ($L \to \infty$) limit. This scaled coupling will be used in the majority of our simulations, and is covered in more detail in Sec. IV. For now, we note that $\gamma \sim L^{-1/2}$ scales to zero faster than the $L^{-1/6}$ that we predict is required for MBL.
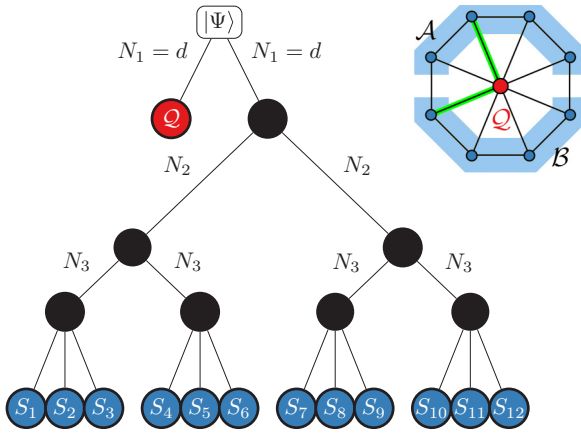
FIG. 2. Expansion of the wave function $|\Psi\rangle$ and the first-layer single-particle functions $|\varphi_{j_\kappa}^{(\kappa)}(t)\rangle$ used in the ML-MCTDH approach (left) and a schematic representation of the tree structure of the wave function (right). The black dots represent single-particle functions (SPFs). The red dot represents the qudit degree of freedom, and the blue dots represent the spin degrees of freedom. The binary expansion of the spin wave function is symmetric, and thus we choose the numbers of SPFs within one layer to be equal. In the example shown, only three spins are grouped together in the lowest layer for better visualization. In the calculation, however, groups of up to 12 spins in the lowest layer are used.

Therefore, at sufficiently late times, we predict MBL with our scaled coupling.

In this model, we use qudits for numerical simplicity due to their finite Hilbert spaces. However, our conclusions can be easily applied also to the case in which the central degree of freedom is a single bosonic mode, such as in cavity QED or superconducting circuits. In these setups, we expect similar dynamical behaviors when the central coupling is appropriately scaled [12].

III. NUMERICAL METHOD

The nonlocal interaction induced by the centrally coupled qudit makes the simulation based on matrix product operator techniques like time-evolving block decimation [25] inefficient. Instead we employ the multilayer multiconfiguration time-dependent Hartree (ML-MCTDH) method [15,16,18,19,26], which has been used to study similar systems in the past, e.g., a two-level system coupled to a bath of noninteracting spins [27]. The ML-MCTDH method generalizes the original MCTDH method [17,28–31] for applications to significantly larger systems. The ML-MCTDH approach represents a rigorous variational basis-set method, which uses a multiconfiguration expansion of the wave function, employing time-dependent basis functions and a hierarchical multilayer representation. Within this framework, the wave function is recursively expanded as a superposition of Hartree products as depicted in Fig. 2. Here, $|\varphi_{j_\kappa}^{(\kappa)}(t)\rangle$, $|v_{i_q}^{(\kappa,q)}(t)\rangle$, ..., are the so-called "single-particle functions" (SPFs) for the first, second, etc. layer, and the coefficients $A_{j_1,...,j_N}$, $B_{i_1,...,i_{Q(\kappa)}}^{\kappa,j_\kappa}$ are the expansion coefficients of the first, second, etc. layer. Despite their name, SPFs describe multiple degrees of freedom; see Fig. 2. The ML-MCTDH equations of motions

for the expansion coefficients and the single-particle functions are obtained by applying the Dirac-Frenkel variational principle [15,32], thus ensuring convergence to the solution of the time-dependent Schrödinger equation upon increasing the number of SPFs. In principle, the recursive multilayer expansion, which corresponds to a hierarchical tensor decomposition in the form of a tensor tree network, can be carried out to an arbitrary number of layers. In practice, the multilayer hierarchy is terminated at a particular level by expanding the single-particle functions in the deepest layer in terms of time-independent basis functions.

In the present application of the ML-MCTDH method, we separate the qudit wave function and the spin-chain wave function in the uppermost layer as depicted schematically in Fig. 2. The wave function of the spin chain is then further expanded in a binary tree (i.e., $P = Q = 2$) up to the lowest layer, which comprises blocks of up to 12 spins. Each of the lowest blocks is expanded in the time-independent local basis of the underlying Hilbert space. Regarding the number of SPFs in the first layer, N_1, it can be shown that $N_1 > d$ leads to redundant configurations in the expansion [28], and thus we set $N_1 = d$ in all calculations. The required number of SPFs in the other layers of the expansion of the spin-chain wave function was determined by thorough convergence tests and depends on the coupling strength γ. In general, fewer SPFs are needed for smaller coupling strengths. For $L = 24$, two dynamical layers are employed, and the required number N_2 of SPFs varies from 30 to 120 SPFs. For $L = 48$, a three-layer scheme is used where the number of SPFs in the lowest layer varies from 10 to 30 and in the highest layer from 20 to 60. For $L = 96$, four layers are employed with SPFs that vary from 10 to 20 in the lowest layer and from 35 to 50 in the highest layer.

IV. RESULTS FOR SCALED COUPLING

We examine the system at infinite temperature by focusing on states in the middle of the many-body spectrum, which have energies close to the midpoint between the maximal and minimal energies of the coupled system ($E_{\max}$ and $E_{\min}$, respectively). We take $\gamma = 0$ for $t < 0$ with the spins in a "super-Néel" state $|\downarrow\downarrow\uparrow\uparrow\cdots\rangle$ and the qudit occupying its middle state $|(d+1)/2\rangle$. The coupling is switched on instantaneously at $t = 0$ to a finite value. The super-Néel state is on average a zero-energy eigenstate of H_0 and has subextensive energy variance, making it a suitable microcanonical probe. Thus, when the system is thermalizing and shows ensemble equivalence, we expect similar dynamics compared to those obtained through averaging over random initial product states, mimicking an infinite-temperature canonical ensemble.

As there are different dynamical behaviors in our model, we shall organize our discussion around the schematic phase diagram in Fig. 1, similar to the one first introduced in [12]. In this first section, we will consider scaling the coupling as $\gamma \sim 1/\sqrt{L}$, corresponding to the three solid lines in the phase diagram, which, from top to bottom, will be referred to as the strong-, intermediate-, and weak-coupling regimes. The orientation of these cuts comes from the $1/\sqrt{L}$ scaling of γ. This is natural if we think of the qudit as our main object of interest, as it gives a well-defined thermodynamic limit for the qudit when it is coupled to a noninteracting bath, such
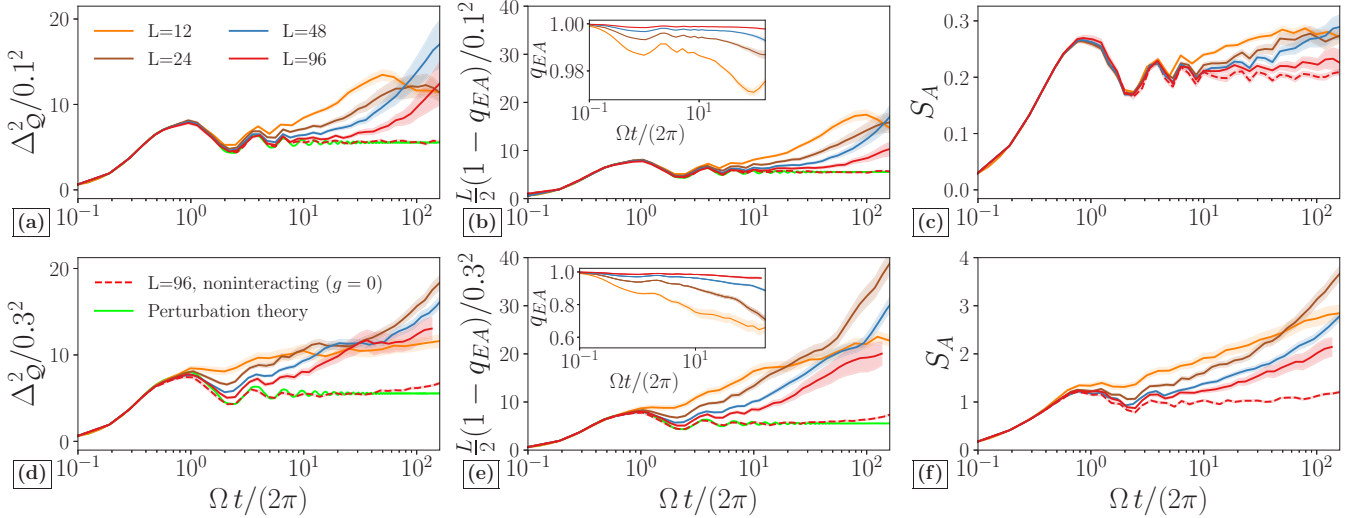
FIG. 3. Dynamics from an initial "super-Néel" state in the regimes of weak (top row, $\gamma = 0.1/\sqrt{L/12}$) and intermediate coupling (bottom row, $\gamma = 0.3/\sqrt{L/12}$). The data are averaged over $O(10^2)$–$O(10^3)$ disorder realizations, with the shaded bands indicating deviations of ± 1 standard error of the mean. Left: Variance of qudit occupations $\Delta_Q^2 = \langle (\tau^z)^2 \rangle - \langle \tau^z \rangle^2$; center: deviation from perfect spin-glass order $1 - q_{EA}$; and right: entanglement entropy S_A between a contiguous half of the spin chain and its complement. The observables Δ_Q^2 and $1 - q_{EA}$ have been appropriately rescaled [24] to show their coincidence (except a factor of 2) at early times for weak coupling. The dynamics are observed to converge to a single curve (green line) and appear to be consistent with the dynamics without the nearest-neighbor Ising coupling (red dashed line) as $L \to \infty$. The data for the noninteracting case are identical for the largest system sizes shown on the timescales of these plots.

as in the spin-boson model [33]. This scaling reproduces the Kac prescription [34] for the all-to-all term in the effective Hamiltonian ensuring also the existence of a thermodynamic limit for the spins. Specifically, we scale γ using the following formula:

$$\gamma = \gamma_0 \sqrt{\frac{L_0}{L}}, \qquad (3)$$

where $L_0 = 12$ throughout for convenience, such that $\gamma = \gamma_0$ at $L = 12$. γ_0 sets the overall strength of the coupling. We will consider three regimes, indicated by the solid lines in Fig. 1: weak coupling ($\gamma_0 = 0.1$), intermediate coupling ($\gamma_0 = 0.3$), and strong coupling ($\gamma_0 = 0.7$).

A. Weak and intermediate coupling (region I)

The first cases we consider are weak and intermediate coupling, which are labeled region I in Fig. 1. These are both at sufficiently small γ_0 that we expect MBL for the largest accessible system sizes, but for intermediate coupling ($\gamma_0 = 0.3$) the system will be near the phase transition for small L. Three observables—the qudit variance Δ_Q^2 [Eq. (4)], the spin glass order parameter q_{EA} [Eq. (5)], and the entanglement entropy of the half-chain S_A [Eq. (6)]—are plotted in Figs. 3 and 4, which correspond to identical data with different scaling of the time axis. The origin of this scaling will be clarified shortly.

Note first that, by preparing both the qudit and the spins in highly excited states, one would normally expect the system to relax quickly to a featureless "infinite-temperature" equilibrium. That is, all internal levels of the qudit should be equally occupied, and the spins should be paramagnetic and translationally invariant. This is not true for the disordered system we study, as the numerics demonstrate in Fig. 3: for sufficiently small coupling, the system shows localization in

both the qudit and its surrounding spins. The former is signaled by the variance of the qudit occupations,

$$\Delta_Q^2 \equiv \langle (\hat{\tau}^z)^2 \rangle - \langle \hat{\tau}^z \rangle^2, \qquad (4)$$

which saturates to a quantity far below that of the uniform limit, $\Delta_Q^2 = (d^2 - 1)/12 = 4$. Furthermore, the different system sizes exhibit scaling collapse of Δ_Q^2 up to a timescale $t \sim 1/\gamma$. This is a property of the scaled γ, as it implies that the spin chain acts as a bath for the qudit with a well-defined thermodynamic limit. More specifically, it can be shown that the considered model with scaled coupling $\gamma \propto L^{-1/2}$ fulfills linear response in the thermodynamic limit, meaning that the effect of the spin environment on the qudit is captured by the first two cumulants of the influence functional [35–37]. For our model, the first cumulant vanishes and thus the reduced qudit dynamics is determined by the second cumulant, given by the force-force autocorrelation function of the spin chain. This also means that one can construct an effective harmonic bath whose correlation function is the same as that of the spin chain resulting in the same reduced qudit dynamics [36]. For our model, the effective harmonic bath is characterized by a spectral density that depends in general on the initial state, the random local fields, and the spin-spin coupling g. For the specific initial state considered here, the spectral density of the effective harmonic bath is equal to the probability distribution of twice the random local fields, and thus is independent of g.

Having established scaling collapse of the qudit variance, we now turn our attention to the dynamics of the spin chain, starting with the spin-glass order parameter

$$q_{EA}(t) \equiv L^{-1} \sum_i \langle \psi | \sigma_i^z(t) \sigma_i^z(0) | \psi \rangle. \qquad (5)$$

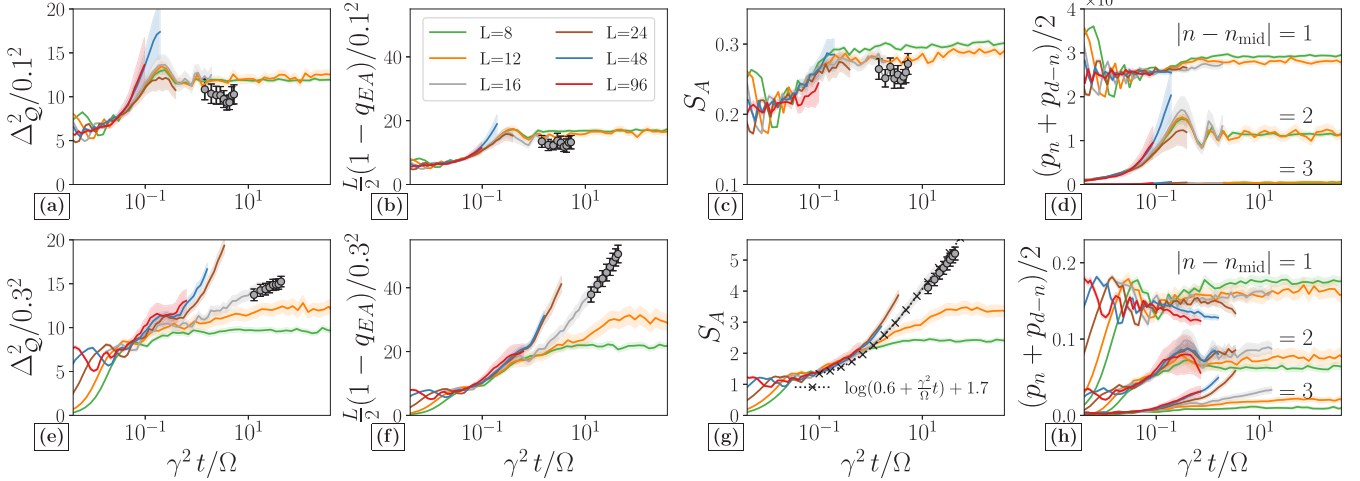Unlike the qudit variance, the spin-glass order parameter displays marked drifts with system size [see the insets of

FIG. 4. Same as in Fig. 3, but with time rescaled by the system size-dependent coupling γ. Gray dots are independent calculations using the kernel polynomial method, aimed to extend the maximum time from $\Omega t/(2\pi) \sim 6 \times 10^2$ to $\Omega t/(2\pi) \sim 1.9 \times 10^3$. Between the weak-coupling [(a)–(d)] and intermediate-coupling [(e)–(h)] regimes, there is a qualitative shift in the long-time behavior of both the qudit- and spin-only observables. These data are suggestive of logarithmic growth in the entanglement entropy becoming the dominant characteristic after $t \sim 1/\gamma^2$. (d),(h) Occupations p_n of the qudit levels, symmetrized around the middle level $|n_{\text{mid}}\rangle = |4\rangle$. While both the weak-coupling [(d)] and intermediate-coupling [(h)] regimes have most of their populations concentrated the initial occupied level, $|4\rangle$, the latter case has a much greater fraction of the total population in the extremes of the qudit's states. The values of p_n for $|n - n_{\text{mid}}| = 3$ in the upper right panel are too small [$\sim O(10^{-4}$–$10^{-3})$] for the scale.

Figs. 3(b) and 3(e)]. The tendency of $q_{\text{EA}}(t) \to 1$ comes from our choice of scaling γ, since γ controls the strength of a local transverse field and thus governs the rate and magnitude of a single spin's precession. On reachable timescales $t \lesssim 10^2$, the largest system size $L = 96$ has near perfect memory of the initial state. This behavior is consistent with our claim that the scaling of $\gamma \sim 1/\sqrt{L}$ toward zero with increased system size is sufficiently fast that the system will flow to MBL for arbitrary γ_0, although proving MBL would require evolution to much later times than we can access.

Though the usefulness of the influence functional approach is restricted to the qudit, we should—by virtue of the fact that the initial spin dynamics are driven by interactions with the qudit (for initial product states like the super-Néel state we have chosen)—find that the spin observables are linked to the qudit's. The spin observables should therefore enjoy a similar limiting behavior to $\gamma \propto L^{-1/2} \to 0$. We indeed show this to be the case within first-order perturbation theory. In [24], we perform time-dependent perturbation theory using the method of multiple scales. We solve for the time evolution operator perturbatively by introducing new "independent" timescales t, $t' \equiv \gamma t$, $t'' \equiv \gamma^2 t$, ..., which allow for control over secular terms growing with t. In the thermodynamic limit with scaled coupling, we find that the dynamics of the qudit are described perturbatively to first order up to time $O(1/\gamma)$ (dotted lines in Fig. 3), providing a complementary approach to the linear-response solution from the influence functional formalism. The perturbative calculation also demonstrates that spin observables should exhibit similar gradual convergence to a single limit up to timescales $t \sim O(1/\gamma)$. Remarkably, the connection between qudit variance and the spin-glass order parameter is even more precise in this limit; they collapse to a single, universal curve in the thermodynamic limit upon

scaling as Δ_Q^2/γ_0^2 and $(1 - q_{\text{EA}})L/(2\gamma_0^2)$, as seen in Figs. 3(a), 3(b), 3(d), and 3(e). Physically, this comes from the fact that a single perturbative excitation of the qudit through the $\hat{\tau}^+ + \hat{\tau}^-$ component of H_1 gives a single spin-flip excitation of the spin chain through σ_j^x.

Finally, we consider the entanglement entropy

$$S_A = -\text{Tr}(\rho_A \log_2 \rho_A) \qquad (6)$$

between a contiguous half of the spins with the rest of the system, which is a defining feature in many-body localization. Here ρ_A is the reduced density matrix of half of the spin system, e.g., sites 1 through $L/2$. As with the previous two quantities, there appears to be a gradual convergence of S_A to a universal curve with increasing L, although unlike the other observables, the entanglement depends on the strength of the coupling prefactor γ_0. By turning off the Ising interaction g (dashed lines in Fig. 3), we see that the dynamics of entanglement at short times $\lesssim O(1)$ are unchanged—as predicted from time-dependent perturbation theory—while growth of entanglement at intermediate times is dependent on this $\sigma_i^z \sigma_{i+1}^z$ interaction.

These observations about the short-time dynamics hold for both weak and intermediate coupling, as seen in Fig. 3. However, we can identify a slower timescale beyond $t \lesssim O(1/\gamma)$ from first-order perturbation theory, on which the Ising interactions start to play a role. In Fig. 4, the same data are plotted upon rescaling the time by t/γ^{-2}. The observables are seen to roughly collapse for both the weak and intermediate couplings and, for intermediate couplings, entanglement in particular shows interesting intermediate-time behavior. While the collapse is imperfect, we note a few salient features. First, deep in the localized (weak-coupling) regime, the spread of the

qudit occupation, the growth of bipartite entanglement entropy, and the decay of the spin-glass order parameter appear to be arrested at long times. It is unclear whether the observables will continue to grow at later times, but our data leave open the possibility that they saturate and that the asymptotic value may be system-size-independent under the chosen scaling. Second, the dynamics of the qudit appear to be correlated with the dynamics of the spins, albeit with a slight time delay. Finally, in the intermediate-coupling regime, the entanglement entropy continues to grow at late times. For $L = 16$, there appears to be a logarithmic growth over three decades in rescaled time [see Fig. 4(g)]. The same may be true for $L \geqslant 24$, but we have insufficient data to decisively prove slow growth over several decades. As seen in Fig. 4(h), the period of potentially logarithmic growth coexists with the period of finite occupation in the edge of the qudit spectrum (states $n = 1$ and d), for which the high-frequency expansion yields all-to-all interactions [see Eq. (2)].

It is unclear what drives the logarithmic behavior. When focusing on the bipartite entanglement entropy, two generic mechanisms have been studied in recent years: the slow dephasing from a quench due to interactions between exponentially localized (quasilocal) operators [38,39], and the linearly diverging semiclassical trajectories of the collective spin state [40] in long-ranged interacting spin systems. In the former case, it has been found that the slope of the logarithmic growth is independent of the strength of interactions [41]. This does not appear to be the case in our numerics, with the larger system sizes $L \geqslant 24$ ostensibly displaying log growth with a larger prefactor than in the $L = 16$ case. Moreover, there does not appear to be any logarithmic trend when the system is deep in the localized phase (see the top row of Fig. 4). If conserved quasilocal operators do exist in this system, then our results would suggest that their localization lengths are strongly dependent on the coupling γ.

Another possibility for the appearance of logarithmic growth of S_A could come from the mediated all-to-all interactions predicted in the effective Hamiltonian [Eq. (2)]. In our qudit system, long-ranged interactions begin to play a significant role when the extremal states of the qudit are occupied (see the discussion in Sec. II). It was argued that these mediated interactions are responsible for the localization-delocalization transition upon decreasing $d/\sqrt{L}$, shown in Fig. 1. Consistent with this, we see significantly greater occupation in the extremal qudit states for intermediate couplings—where logarithmic growth is seen—compared to weak couplings [see Figs. 4(d) and 4(h)]. It is also clear that the slow growth of Δ_Q^2 for intermediate couplings is due in part to the slow growth in the occupations of the $|1\rangle$ and $|7\rangle$ states.

Regardless of the origin of slow growth, finite occupation at the extremes of the qudit spectrum implies a departure from the Floquet regime. Our finite-time numerics are unable to resolve whether this implies delocalization. Should this mechanism give rise to a sharp localization transition, it would possibly be of a different character from the extensively studied MBL transition based on ergodic grains thermalizing nearby insulating regions through short-range interactions [42–45].
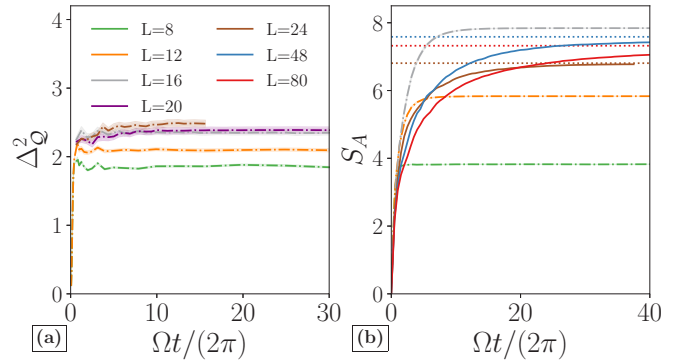

FIG. 5. Dynamics for strong coupling, $\gamma = 0.7/\sqrt{L/12}$. (a) Qudit variance Δ_Q^2 and (b) bipartite entanglement entropy S_A. Results from ML-MCTDH are not included for Δ_Q^2 as they are not converged. For system sizes where the dynamics can be computed exactly (dot-dashed lines), S_A saturates the Page bound $S_A \sim L/2$. The curves from ML-MCTDH (solid lines), corresponding to $L \geqslant 24$, saturate the bound set by the number of single-particle functions in the second layer, $\log_2 \chi_2$ (dotted lines).

B. Strong coupling (region II)

In the strong-coupling regime (Fig. 5), our phase diagram suggests that the system lies deep within the thermalizing phase for our available system sizes due to strong delocalizing interactions between the spins induced by the central qudit. Our data are consistent with this expectation, but we note two effects. First, despite the fact that spins thermalize, we observe that the asymptotic distribution of qudit occupations is nonuniform, similar to the athermal qudit regime found in [12]. In Sec. IV of [24] we introduce a phenomenological picture to explain this based on random matrix theory, suggesting that it is rare for the qudit to make transitions between widely separated states.

Second, we note that due to the ergodic character of the dynamics in the strong-coupling thermalizing regime, the accurate treatment of the dynamics represents a significant challenge for the ML-MCTDH approach and cannot be converged for longer times [46]. This well-known limitation of the ML-MCTDH method and other tensor network approaches is due to the following reason. Within the ML-MCTDH approach, the wave function of the system is represented in each layer by sums of Hartree products, the total number of which is determined by the number N_n of SPFs employed in a given layer n for each degree of freedom. For example, in the binary tree depicted in Fig. 2, N_2 SPFs are used in the second layer to represent each of the two parts of the spin chain resulting in $(N_2)^2$ Hartree products that represent the spin system in the second layer. As a consequence, the entanglement entropy between the different constituents of the system is bounded by $\log N_2$. However, for ergodic systems, the entanglement entropy is extensive, and thus, starting from an uncorrelated state, the entanglement entropy grows and eventually exceeds the limit of $\log N_2$. This implies that, for longer times, the wave function of the system cannot be represented accurately. The application of the ML-MCTDH formalism in the ergodic phase is thus restricted to short times. Therefore, the results for the qudit variance depicted in Fig. 5

have been obtained by exact diagonalization and the kernel polynomial method.

Despite this limitation of ML-MCTDH, we are still able to find signatures of thermalization by examining the dependence of the dynamics on N_2. In the right panel of Fig. 5, we see that the bipartite entanglement entropy is upper bounded by $\log_2 N_2$, corresponding to a maximal entropy state within our variational ansatz. We observe a similarly strong dependence of q_{EA} when increasing N_2, which drifts toward zero to indicate paramagnetic behavior in the spin chain. Other observables, such as the populations of the qudit levels, cannot be converged, implying that information about the ergodic state is present but limited.

V. RESULTS FOR UNSCALED COUPLING

The dynamics of our system with scaled coupling, $\gamma \sim 1/\sqrt{L}$, is perhaps most interesting because it gives a well-defined thermodynamic limit for the qudit. However, it is also important to understand the dynamics when the coupling is held fixed instead of being scaled by system size, corresponding to the dashed horizontal line in Fig. 1. Fixing the coupling strength may be easier to implement experimentally, for example in cavity QED where the coupling is governed by the position-dependent electric field strength. Doing so, however, means that we can no longer easily separate dynamics occurring on different timescales as in the previous section. Furthermore, we predict that in the thermodynamic limit this will eventually result in thermalization, as the long-range interactions induced by the central qudit will eventually dominate at large enough times and system sizes. We choose the fixed value $\gamma = 0.106\,07$, which precisely matches the intermediate scaled coupling for our largest system size, and therefore lives within the predicted MBL phase for all accessible system sizes.

The dynamics with fixed coupling, shown in Fig. 6, looks similar to the data at intermediate scaled coupling but without as clear a separation of timescales or data collapse. We note that it is harder to detect the sort of logarithmically slow delocalization as seen in q_{EA} in Fig. 4(f) [cf. Fig. 6(a)]. The story is the same with the qudit variance, which is similar to $1 - q_{EA}$ when divided by L. However, with the fixed coupling, the entanglement entropy reflects a qualitative change in behavior at large enough system sizes.

We see that at times $\frac{\Omega}{2\pi} t \sim 6 \times 10^1$ in the localized phase (Fig. 6), the smaller system sizes $L \leqslant 16$ establish a subextensive amount of entanglement entropy. Numerics from ML-MCTDH seem to counter this trend, with S_A continuing to grow slowly beyond this timescale. The rate of this growth increases with L, which is consistent with it arising from stronger effective all-to-all interactions described by the high-frequency expansion [Eq. (2)]. It also appears to show strong system size dependence at short times, where a subextensive amount of entanglement is established. This should be contrasted with models of MBL without central coupling, in which the short-time behavior is system-size-independent.

As a final note, we point out that the entanglement entropy at fixed γ is subextensive, such that S_A/L appears to be trending toward zero with increasing system size. This should be contrasted with mutual information between the two halves of
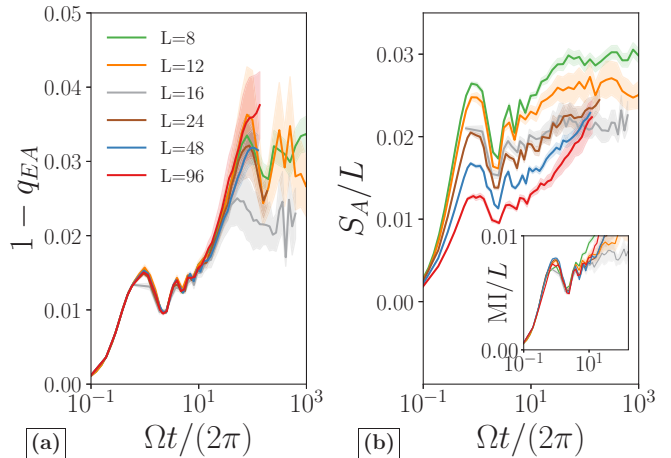

FIG. 6. Dynamics with unscaled coupling, $\gamma = 0.106\,07$. On the reachable timescales, the spin-glass order parameter q_{EA} (a) does not show a significant system size dependence. However, the bipartite entanglement entropy (b), in addition to being subextensive—$S_A \propto L^\alpha$, $0 < \alpha < 1$—at short times, already shows qualitatively different behavior at intermediate time for $L \gtrsim 24$. Inset: Mutual information MI $\equiv I(A, B)$ between two contiguous halves A and B of the spin chain (see the main text).

the spin chain,

$$I(A, B) = S(A) + S(B) - S(A \cup B),$$

which is extensive. In Ref. [12], mutual information was used as a proxy for entanglement between the two halves of the spin chain, as it nominally removes "unimportant" entanglement with the central qudit. However, since entanglement must be subextensive—indeed, system-size-independent—in the MBL phase, our data indicate that entanglement entropy is a better metric than mutual information for capturing this. Our initial expectation was that mutual information would become subextensive at larger system size, but the results obtained with the ML-MCTDH method rule out that possibility.

VI. CONCLUSIONS

In this paper, we have studied the dynamical behavior of a qudit coupled to a disordered, interacting bath of up to $L = 96$ spins-1/2, which altogether can exhibit localization at strong disorder. Using a combination of exact propagation methods and the tensor network-based ML-MCTDH approach, we find evidence of qualitatively different dynamical signatures in local observables such as the spin-glass order of the bath and the qudit variance, consistent with a rough phase diagram (Fig. 1). Most notably, we find hints of logarithmically slow decay of localization near the onset of all-to-all interactions in the bath. This behavior was found to occur after timescales $t \sim O(1/\gamma^2)$, where γ is the qudit-spin bath coupling.

The behavior of the qudit observed here is, we believe, not specific to this model. Our conclusions should apply equally well to the cases of a cavity photon with rescaled raising/lowering operators $a^\dagger \rightarrow (N_0)^{-1/2} a^\dagger$ or central spin-S systems with operators rescaled as $\hat{S} \rightarrow [S(S-1)]^{-1/2}\hat{S}$. The feature of these systems is that the fundamental commutation

relation between the raising and lowering operators vanishes in the limit of large S or large N_0. This fact allows for exact cancellation between processes that raise or lower the qudit state. However, this mechanism only serves to protect localization for sufficiently large "magnetic field" Ω; it is unclear how these systems interpolate between the $\Omega = 0$ limit and the $\Omega > |g|, |h_i|, \ldots$ limit. We note additionally that the limitations of ML-MCTDH for these types of centrally coupled systems with many-body interacting baths in the strong-coupling regime require more clarification. Such clarification may be necessary to extend the effectiveness of the method into the thermalizing regime on the left side of the phase diagram 1, which remains numerically inaccessible and thus poorly understood.

[1] A. Blais, R.-S. Huang, A. Wallraff, S. M. Girvin, and R. J. Schoelkopf, Phys. Rev. A **69**, 062320 (2004).

[2] E. J. Davis, G. Bentsen, L. Homeier, T. Li, and M. H. Schleier-Smith, Phys. Rev. Lett. **122**, 010405 (2019).

[3] K. Xu, J.-J. Chen, Y. Zeng, Y.-R. Zhang, C. Song, W. Liu, Q. Guo, P. Zhang, D. Xu, H. Deng, K. Huang, H. Wang, X. Zhu, D. Zheng, and H. Fan, Phys. Rev. Lett. **120**, 050507 (2018).

[4] J. Z. Imbrie, J. Stat. Phys. **163**, 998 (2016).

[5] D. A. Huse, R. Nandkishore, V. Oganesyan, A. Pal, and S. L. Sondhi, Phys. Rev. B **88**, 014206 (2013).

[6] V. Khemani, Ph.D. thesis, Princeton (2016).

[7] N. Y. Yao, C. R. Laumann, S. Gopalakrishnan, M. Knap, M. Müller, E. A. Demler, and M. D. Lukin, Phys. Rev. Lett. **113**, 243002 (2014).

[8] A. O. Maksymov and A. L. Burin, Phys. Rev. B **101**, 024201 (2020).

[9] R. Nandkishore, S. Gopalakrishnan, and D. A. Huse, Phys. Rev. B **90**, 064203 (2014).

[10] D. A. Abanin, W. D. Roeck, and F. Huveneers, Ann. Phys. **372**, 1 (2016).

[11] P. Ponte, Z. Papić, F. Huveneers, and D. A. Abanin, Phys. Rev. Lett. **114**, 140401 (2015).

[12] N. Ng and M. Kolodrubetz, Phys. Rev. Lett. **122**, 240402 (2019).

[13] P. Ponte, C. R. Laumann, D. A. Huse, and A. Chandran, Philos. Trans. R. Soc. A **375**, 20160428 (2017).

[14] D. Hetterich, N. Y. Yao, M. Serbyn, F. Pollmann, and B. Trauzettel, Phys. Rev. B **98**, 161122(R) (2018).

[15] H. Wang and M. Thoss, J. Chem. Phys. **119**, 1289 (2003).

[16] U. Manthe, J. Chem. Phys. **128**, 164116 (2008).

[17] H.-D. Meyer, F. Gatti, and G. Worth, *Multidimensional Quantum Dynamics* (Wiley-VCH, Weinheim, 2009).

[18] O. Vendrell and H.-D. Meyer, J. Chem. Phys. **134**, 044135 (2011).

[19] H. Wang, J. Phys. Chem. A **119**, 7951 (2015).

[20] M. Schreiber, S. S. Hodgman, P. Bordia, H. P. Lüschen, M. H. Fischer, R. Vosk, E. Altman, U. Schneider, and I. Bloch, Science **349**, 842 (2015).

[21] P. Roushan, C. Neill, J. Tangpanitanon, V. M. Bastidas, A. Megrant, R. Barends, Y. Chen, Z. Chen, B. Chiaro, A. Dunsworth, A. Fowler, B. Foxen, M. Giustina, E. Jeffrey, J. Kelly, E. Lucero, J. Mutus, M. Neeley, C. Quintana, D. Sank, A. Vainsencher, J. Wenner, T. White, H. Neven, D. G. Angelakis, and J. Martinis, Science **358**, 1175 (2017).

[22] P. Sierant, K. Biedroń, G. Morigi, and J. Zakrzewski, SciPost Phys. **7**, 8 (2019).

[23] This estimate is subject to strong finite-size effects.

[24] See Supplemental Material at http://link.aps.org/supplemental/10.1103/PhysRevB.103.134201 for a discussion on the cumulant expansion, an ansatz for the steady state of the thermalizing phase, and perturbation theory using multiple scales, which includes Refs. [37,47–49].

[25] S. Paeckel, T. Köhler, A. Swoboda, S. R. Manmana, U. Schollwöck, and C. Hubig, Ann. Phys. **411**, 167998 (2019).

[26] G. Worth, M. H. Beck, A. Jäckle, O. Vendrell, and H.-D. Meyer, The MCTDH Package, Version 8.5.11 (2019); see http://mctdh.uni-hd.de.

[27] H. Wang and J. Shao, J. Chem. Phys. **137**, 22A504 (2012).

[28] H.-D. Meyer, U. Manthe, and L. Cederbaum, Chem. Phys. Lett. **165**, 73 (1990).

[29] U. Manthe, H.-D. Meyer, and L. S. Cederbaum, J. Chem. Phys. **97**, 3199 (1992).

[30] M. Beck, A. Jäckle, G. Worth, and H.-D. Meyer, Phys. Rep. **324**, 1 (2000).

[31] H.-D. Meyer, Wiley Interdiscip. Rev.: Comput. Mol. Sci. **2**, 351 (2012).

[32] H. Wang and M. Thoss, J. Chem. Phys. **131**, 024114 (2009).

[33] U. Weiss, *Quantum Dissipative Systems* (World Scientific, Singapore, 2012).

[34] M. Kac, G. E. Uhlenbeck, and P. C. Hemmer, J. Math. Phys. **4**, 216 (1963).

[35] R. Feynman and F. Vernon, Ann. Phys. **24**, 118 (1963).

[36] N. Makri, J. Phys. Chem. B **103**, 2823 (1999).

[37] H. Wang and M. Thoss, J. Phys. Chem. A **111**, 10369 (2007).

[38] M. Žnidarič, T. Prosen, and P. Prelovšek, Phys. Rev. B **77**, 064426 (2008).

[39] D. A. Abanin, E. Altman, I. Bloch, and M. Serbyn, Rev. Mod. Phys. **91**, 021001 (2019).

[40] A. Lerose and S. Pappalardi, Phys. Rev. Research **2**, 012041(R) (2020).

[41] J. A. Kjäll, J. H. Bardarson, and F. Pollmann, Phys. Rev. Lett. **113**, 107204 (2014).

[42] R. Vosk and E. Altman, Phys. Rev. Lett. **110**, 067204 (2013).

[43] P. T. Dumitrescu, R. Vasseur, and A. C. Potter, Phys. Rev. Lett. **119**, 110604 (2017).

[44] A. Goremykina, R. Vasseur, and M. Serbyn, Phys. Rev. Lett. **122**, 040601 (2019).

[45] A. Morningstar, D. A. Huse, and J. Z. Imbrie, Phys. Rev. B **102**, 125134 (2020).

[46] T. Westermann and U. Manthe, J. Chem. Phys. **136**, 204116 (2012).

[47] J. Shao and P. Hänggi, Phys. Rev. Lett. **81**, 5710 (1998).

[48] A. Lucas, arXiv:1903.01468.

[49] P. Hauke and M. Heyl, Phys. Rev. B **92**, 134204 (2015).